Assessing the role of the active-site cysteine ligand in the superoxide reductase from Desulfoarculus baarsii.

Christelle Mathé, Claire O Weill, Tony A Mattioli, Catherine Berthomieu, Chantal Houée-Levin, Emilie Tremey, Vincent Nivière

ASSESSING THE ROLE OF THE ACTIVE-SITE CYSTEINE LIGAND IN THE SUPEROXIDE REDUCTASE FROM *DESULFOARCULUS BAARSII**

Christelle Mathé [‡§], Claire O. Weill [‡†], Tony A. Mattioli [§], Catherine Berthomieu [#], Chantal Houée-Levin [¶], Emilie Tremey [‡] and Vincent Nivière [‡]

[‡] Laboratoire de Chimie et Biologie des Métaux, iRTSV-CEA Grenoble/CNRS/Université Joseph Fourier, 17 Avenue des Martyrs, 38054 Grenoble Cedex 9, France. [§] Laboratoire de Stress Oxydant et Détoxication, SB^{2}SM, iBiTec-S, CEA Saclay/CNRS, 91191 Gif-sur-Yvette cedex, France. [#] Laboratoire des Interactions Protéine Métal, SBVME-CEA Cadarache/CNRS/Université Aix-Marseille II, 13108 Saint-Paul-lez-Durance Cedex, France. [¶] Laboratoire de Chimie Physique, CNRS/Université Paris-Sud, Bâtiment 350, Centre Universitaire 91405 Orsay Cedex, France. [†] Present address: Polyplus-Transfection, Bioparc BP 90018, Boulevard Sébastien Brandt, 67401 Illkirch Cedex, France.

Running Title: Function of the cysteine axial ligand in SOR activity.

Christelle Mathé and Claire O. Weill contributed equally to this work.
Address correspondence to: V. Nivière, Tel.: 33-4-38-78-91-09; Fax: 33-4-38-78-91-24; E-mail: vniviere@cea.fr

Superoxide reductase is a novel class of non-heme iron proteins that catalyzes the one-electron reduction of $O_2^{\bullet-}$ to H_2O_2, providing an antioxidant defense in some bacteria. Its active site consists of an unusual non-heme Fe^{2+} center in a [His_4 Cys_1] square pyramidal pentacoordination. In this class of enzyme, the cysteine axial ligand has been hypothesized to be an essential feature in the reactivity of the enzyme. Previous Fourier transform infrared spectroscopy studies on the enzyme from *Desulfoarculus baarsii* revealed that a protonated carboxylate group, proposed to be the side chain of Glu114, is in interaction with the cysteine ligand. In this work, using pulse radiolysis , Fourier transform infrared and resonance Raman spectroscopies, we have investigated to what extent the presence of this Glu114 carboxylic lateral chain affects the strength of the S-Fe bond and the reaction of the iron active site with superoxide. The E114A mutant shows significantly modified pulse radiolysis kinetics for the protonation process of the first reaction intermediate. Resonance Raman spectroscopy demonstrates that the E114A mutation results in both a strengthening of the S-Fe bond and an increase in the extent of freeze-trapping of a Fe-peroxo species after treatment with H_2O_2 by a specific strengthening of the Fe-O bond. A fine tuning of the strength of the S-Fe bond by the presence of Glu114 appears to be an essential factor for both the strength of the Fe-O bond and the pK_a value of the Fe^{3+}-peroxo intermediate species to form the reaction product H_2O_2.

Superoxide reductase (SOR) catalyzes the one-electron reduction of $O_2^{\bullet-}$ to H_2O_2, providing an antioxidant defense in some anaerobic or microaerophilic bacteria (1-5):

$$O_2^{\bullet-} + 1e^- + 2H^+ \rightarrow H_2O_2$$

Historically, the only enzymes known to eliminate superoxide were superoxide dismutases (SODs), which catalyze the disproportionation of superoxide (6). The recently discovered SOR activity involving the reduction of superoxide has changed our view of how toxic superoxide is eliminated in cells and how this activity protects the cell against oxidative stress and lethal levels of superoxide.

SORs are a novel class of non-heme iron proteins that can be classified into one-iron proteins, which possess only the active-site iron center (called Center II) (7-12), and two-iron proteins (2, 13, 14), which possess an additional rubredoxin-like Fe^{3+}-$(SCys)_4$, center (called Center I) for which the function and role are not known (9, 15). In the reduced state, the SOR active site consists of a non-heme Fe^{2+} center in an unusual [His_4 Cys_1] square pyramidal pentacoordination (7, 13, 14). The sixth coordination site of the Fe^{2+} center is vacant and suggests the most obvious site for $O_2^{\bullet-}$ binding. The SOR active site Fe^{2+} center reacts specifically at nearly diffusion-controlled rates with $O_2^{\bullet-}$ according to an inner sphere mechanism (16-21). Although one or two reaction intermediates have been proposed depending on the enzyme studied, it is now generally accepted that these intermediate species are Fe^{3+}-peroxo species (16-24). For the *Desulfoarculus baarsii* enzyme, the reaction mechanism was proposed to involve formation of two intermediates (Scheme 1) (16, 19). The first one, a proposed Fe^{3+}-peroxo species, results from the bimolecular reaction of $O_2^{\bullet-}$ with Fe^{2+}. It then undergoes a diffusion limited protonation process to form a second reaction intermediate, a Fe^{3+}-hydroperoxo species (19). A second protonation process at the level of the Fe^{3+}-hydroperoxo species would allow the release of the reaction product H_2O_2. Although the donor of this second protonation event is not known yet, it was proposed to be associated with the presence of a water molecule at the SOR active site (25). Finally, the resulting Fe^{3+} atom of the active site becomes hexacoordinated with a conserved glutamate residue, Glu47 in *D. baarsii* (Scheme 1) (7, 26).

The strictly conserved cysteine axial ligand in the SOR active site has been hypothesized for long to be an essential feature in the reactivity of the enzyme with superoxide (5, 8). It was also proposed that, similarly to that reported for cytochrome P450 enzymes, rubredoxins or ferredoxins (27-29), H-bonds on the cysteine ligand could finely tune the strength of the Fe-S bond and then, in the case of SOR, might play important role in the reactivity of SOR with superoxide (30). Two peptide NH groups from the Leu/Ile and His of the well conserved tetrapeptide Cys116-Asn117-Leu/Ile118-His119 (numbered according to the *D. baarsii* SOR sequence), are within H-bonding distance of the cysteine ligand sulfur. In the case of the SOR from *D. baarsii*, for which a crystal structure was determined at 1.15 Å resolution (14), the Ile118 and His119 peptide N atoms are at 3.41, and 3.26 Å, respectively, from the cysteine sulfur ligand, suggesting relatively weak H-bonds from these two potential donors (Figure 1). However, up to now, no experimental data have been reported to investigate the functional role of this cysteine residue. Site-directed mutagenesis at this position (Cys → Ala) in the case of *Archaeoglobus fulgidus* SOR enzyme was reported (11) to result in an apoprotein, and thus not suitable for any study of the reaction with superoxide.

In the case of the *D. baarsii* enzyme, redox-induced FTIR difference spectra (exploiting the $Fe^{2+} \rightarrow Fe^{3+}$ redox change at the SOR active site) revealed that a protonated carboxylate group, proposed to be the side chain of Glu114, undergoes conformational modifications upon oxidation of the active-site iron (26). This highlights some marked interaction between this carboxylic group and the iron active site. Glu114 is located near the Cys116 side chain, buried inside the protein in a non-polar environment, compatible with a protonated carboxylate side chain. Its two carboxylic oxygens face directly the S and Fe atoms, with distances of about 5.6-6.5 Å (Figure 1). Such an orientation suggests some dipolar interactions, which could explain the FTIR difference signals. These interactions could also contribute to the modulation of the strength of the S-Fe bond. Glu114 is conserved among the two-iron type of SORs, as well as the one-iron SOR of *Treponema pallidum*. For the *T. pallidum* enzyme, a similar interaction with the iron active site and the lateral chain of a protonated carboxylate was also observed by FTIR spectroscopy (26). On the other hand, most of the one-iron SORs such as the neelaredoxins and as represented by, for example, *Pyrococcus furiosus*, do not have this glutamate residue, where instead a serine residue is found (7). The side chain of this serine residue shows no probable H-bonds donated by the OH group, according to the crystal structure of the *P. furiosus* enzyme (7).

In this work, using pulse radiolysis, FTIR and resonance Raman spectroscopies, we have investigated to what extent the presence of the Glu114 carboxylic lateral chain could affect the strength of the S-Fe bond and the reaction

of the iron active site with superoxide. We report a characterization of the E114A mutant in *D. baarsii* showing significantly modified pulse radiolysis kinetics for the protonation process of the first reaction intermediate. RR spectroscopy shows very local changes at the level of the Fe^{3+}-S(Cys) bond, and demonstrates that the mutant strongly stabilized an iron peroxo species in its active site. This highlights the function of this carboxylic group on the fine tuning of the S-Fe strength and in the role of the cysteine ligand in the reactivity of the enzyme with superoxide.

EXPERIMENTAL PROCEDURES

Materials. For pulse radiolysis experiments, sodium formate and buffers were of the highest quality available (Prolabo Normatom or Merck Suprapure). Oxygen was from ALPHA GAZ. Its purity is higher than 99.99%. Water was purified using an Elga Maxima system (resistivity 18.2 MΩ). K_2IrCl_6 was from Strem Chemical Inc.

Bacterial strain and plasmids. The complementation tests of the *E. coli* QC2375 mutant strain were carried out as previously described (16). Plasmid pMJ25 is a pJF119EH derivative, in which the *sor* gene from *D. baarsii* is under the control of a tac IPTG inducible promotor (2).

Site-directed Mutagenesis and protein purification. Two primers were designed for PCR- based site-directed mutagenesis to create the *D. baarsii* SOR mutant E114A. Primer 1(5'CAAGGTCGTGGCCCGCGCATACTGC AACATCCACG 3') and primer 2 (5' CGTGGATGTTGCAGTATGCGCGGGCCA CGACCTTG 3') contained the mutation of interest (underlined). Mutagenesis was carried out on the plasmid pMJ25 with the QuickChange® site-directed mutagenesis kit from Stratagene. The mutation was verified by DNA sequencing. The resulting plasmid, pCWE114A was transformed in *E. coli* DH5α. Over-expression and purification of the E114A mutant protein was carried out as reported for the wild-type protein (2). The purified mutant protein was found to be as stable as the wild-type protein. The UV-vis absorption spectrum of the purified protein exhibited an A_{280nm}/A_{503nm} ratio of 4.8-4.9 and appeared to be homogeneous, as seen by SDS-PAGE analysis (data not shown). Protein concentration was determined using the Bio-Rad® protein assay reagent. Full metallation of the two mononuclear iron sites was verified by atomic absorption spectroscopy, with a value of 2.0 iron atoms per polypeptide chain (data not shown). The protein was isolated with an oxidized Center I (ε_{503nm} = 4,400 M^{-1} cm^{-1}) and a fully reduced Center II.

pH studies. The following different buffers, at 50 mM, were used to cover the pH range 5.0 to 10.2: pH 5.0 and 5.5, acetate buffer; pH 6.5, 7.0 and 7.5, phosphate buffer; pH 7.6, 8.1 and 8.5, Tris-HCl buffer; pH 9.1, 9.5 and 10.2, glycine-NaOH buffer.

Pulse radiolysis. Pulse radiolysis measurements were performed as described elsewhere (16, 19). Briefly, free radicals were generated by irradiation of O_2-saturated aqueous protein solutions (100 μM), in 10 mM of the different buffers used, 0.1 M sodium formate with 200 ns pulses of 4 MeV electrons at the linear accelerator at the Curie Institute, Orsay, France. Superoxide anion, $O_2^{\bullet-}$, was generated during the scavenging by formate of the radiolytically produced hydroxyl radical, $HO^{\bullet}$, as previously described (16). Doses of ca. 5 Gy per pulse resulted in ca. 3 μM of $O_2^{\bullet-}$. Reactions were followed spectrophotometrically, between 450 and 750 nm, at 20°C in a 2 cm path length cuvette. Kinetic traces were analyzed using a Levenberg-Marquardt algorithm from the Kaleidagraph® software package (Synergy Software).

γ-ray Irradiations. γ-ray irradiations were carried out at 20 °C using a cobalt-60 source, at a dose rate of 5.9 $Gy.min^{-1}$. The SOR protein to be irradiated, 22 μM, was in 10 mM Tris-HCl buffer pH 7.6, 100 mM sodium formate, 500 units/ml of catalase from *Aspergillus niger* and saturated with pure O_2. The duration of irradiation was 6 min (35 Gy) in order to obtain a stoichiometric amount of $O_2^{\bullet-}$ (radiolytic yield 0.62 μmol J^{-1}) relative to SOR.

Resonance Raman. Resonance Raman spectra were recorded using a modified single-stage spectrometer (Jobin-Yvon) equipped with a liquid nitrogen cooled back-thinned CCD detector as described elsewhere (22, 23). Briefly, excitation at 647.1 nm (30 mW) was provided by a Spectra Physics Series 2000 Kr^+ laser. Protein samples were 3-5 mM and in 100-200 mM buffer. A holographic notch filter (Kaiser Optical) was used to reject stray light.

Spectra were calibrated using the exciting laser line, along with the SO_4^{2-} (983 cm^{-1}) and ice (230 cm^{-1}) Raman bands from a frozen aqueous sodium sulphate solution. Spectral resolution was < 3 cm^{-1} with entrance slits at 100 µm and frequency accuracy was ± 1 cm^{-1}. Reported spectra were the result of the averaging of 40 single spectra recorded with 30 seconds of accumulation time. Baseline corrections were performed using GRAMS 32 (Galactic Industries). In all reported spectra, the contributions from ice have been subtracted using the GRAMS 32 software by cancellation of the 230 cm^{-1} band. In general for the resonance Raman samples, 1 µl of concentrated protein (1-5 mM) was deposited on glass slide sample holder and then transferred into a cold helium gas circulating optical cryostat (STVP-100, Janis Research) held at 15 K. For the rapidly frozen H_2O_2-treated Raman samples, 5 µl of concentrated SOR protein (3-6 mM) on ice was manually mixed rapidly with an equal volume of H_2O_2 solution whose concentration was adjusted in order to obtain a final SOR protein: H_2O_2 ratio of *ca*. 1:6 equivalents. 3-5 µL of the resulting mixture were promptly transferred to the glass slide sample holder and immediately immersed in liquid nitrogen before transferring to the optical cryostat for Raman measurement. The entire mixing/freezing operation took no more than ca. 5 seconds.

FTIR. Electrochemically-induced FTIR difference spectra were recorded, using a thin pathlength electrochemical cell and a Bruker 66 SX spectrometer equipped with a KBr beam splitter and a nitrogen-cooled MCT-A detector, as described in (26). 10 µL of a 1 mM solution of SOR in a 50 mM Tris-HCl buffer pH 7.5, 20 mM $MgCl_2$ and 100 mM KCl were used for one sample. Ferrocene, N,N-dimethyl-p-phenylenediamine, 1,4-benzoquinone, N,N,N',N'-tetra-methyl-p-phenylenediamine, 2,3,4,5-tetramethyl-p-phenylenediamine, phenazine ethosulfate, and duroquinone were used as electrochemical mediators, at concentrations of 40 µM.

Optical absorbance measurements were made using a Varian Cary spectrophotometer, in 1 cm path length cuvettes. Low temperature (4.2 K) X-band EPR spectra were recorded on a Bruker EMX 081 spectrometer equipped with an Oxford Instrument continuous flow cold He gas cryostat.

RESULTS

Spectroscopic characterization of the SOR E114A mutant.

The UV-visible absorption spectrum of the as-isolated E114A mutant exhibited the characteristic absorption bands at 370 nm and 503 nm, arising from the ferric iron of Center I (2); these values are similar to those observed for the wild-type protein (2). When treated with a slight excess of K_2IrCl_6, the spectrum of the mutant exhibited an increase in absorbance in the 500-700 nm range, reflecting oxidation of the Center II iron atom (19). The well-defined absorption band corresponding to the oxidized Center II band can be more easily seen when the intense contributions of Center I are subtracted (Figure 2). The maximum of this absorption band strongly depends on the pH, as was determined for the wild-type SOR protein (19). At pH 7.6, in the E114A mutant protein, the band corresponding to the oxidized Center II is centered at 630 nm, with a molar extinction coefficient value of 1,660 mM^{-1} cm^{-1}. Upon increasing the pH from 5 to 10.2, the Center II absorption band shifts from 632 to 547 nm (Figure 2), with an apparent pK_a value of 8.8±0.1 (Inset Figure 2). This pK_a value of the so-called "alkaline transition" is similar to that found for the wild-type (pK_a = 9.0±0.1) (19) and corresponds to the displacement of the glutamate 47 ligand by a hydroxide ion at basic pH values on the sixth coordination position of the active-site ferric iron (25). However, in the case of the E114A mutant, the absorption maxima of the Fe^{3+}-Glu (632 nm) and the Fe^{3+}-OH (547 nm) forms are blue shifted from 12-13 nm compared to that reported for the wild-type protein (644 and 560 nm, respectively) (19). This might reflect some electrostatic changes at or near Center II in the mutant protein.

The 4 K EPR spectra of as-isolated E114A mutant displayed resonances at g = 7.7, 5.7, 4.1 and 1.8, similar to those obtained for the wild-type SOR (2) (data not shown). These resonances are typical of those of a Fe^{3+} ion in a distorted tetrahedral FeS_4 center and originated from Center I (2). The 4 K EPR spectrum of the E114A mutant oxidized with a slight excess of K_2IrCl_6 exhibited an additional signal at g = 4.3 (Figure 3), identical to that observed for wild-type SOR (2). This g=4.3 signal was attributed to the oxidized Center II,

with a rhombic (E/D=0.33) high-spin (S=5/2) ferric ion (2, 30).

For the wild-type protein, FTIR difference spectra for reduced and oxidized iron Center II showed bands at 1770 and 1760 cm^{-1}, respectively (Figure 4, thin line and (26)), assigned to the carbonyl stretching mode, ν(C=O), of a protonated carboxylate group of an Asp or Glu side chain located in a non polar environment (26). The comparison of reduced *minus* oxidized FTIR difference spectra of the wild-type SOR (Figure 4, thin line) with that of the E114A mutant (thick line) clearly indicates that the 1770/1760 cm^{-1} differential signal is not observed when Glu114 is replaced with alanine, a residue which does not possess a carboxylic group. Thus, Glu114, located in a hydrophobic protein environment at ≈ 6 Å of the iron Center II accounts for the 1770/1760 cm^{-1} differential signal (26). Bands at 1200 (oxidized) and 1188 (reduced) cm^{-1} (Figure 4, thin line) can be also assigned to the Glu114 side chain ν(C-O) stretching mode.

In addition, Figure 4 further shows that only modest global protein structural changes are induced by the E114A mutation. Slight spectral changes are observed in the region where peptide ν(C=O) and ν(CN)+(NH) modes contribute, at 1700-1610 and 1580-1520 cm^{-1}, respectively. The infrared bands at 1109 (reduced), 1098 (oxidized) cm^{-1}, assigned to the ring mode of histidine ligands of the iron, remain unchanged for the mutant.

Reaction of E114A SOR with $O_2^{\bullet-}$. Formation of reaction intermediates.

The reaction of the SOR E114A mutant protein with $O_2^{\bullet-}$ was studied by pulse radiolysis. The kinetics of the reaction were followed spectrophotometrically between 450 and 700 nm. The protein was present in large excess with regard to superoxide ([protein] = 20-100 µM, $[O_2^{\bullet-}]$ = 3 µM), and therefore pseudo first-order conditions could be assumed. Kinetics were always analyzed at different wavelengths, which gave qualitatively identical results. As described for the wild-type protein, at pH 7.6 (Refs 16, 19 and Scheme 1), a first reaction intermediate species was formed very rapidly, ca. 50 µs after the pulse, with a first order rate constant (k_1) directly proportional to the protein concentration (data not shown). A second-order rate constant for the reaction of the mutant protein with $O_2^{\bullet-}$ was determined to be $(1.2\pm0.2)\times10^9$ M^{-1} s^{-1}. This value is almost identical to that reported for the wild-type protein (20). Furthermore, k_1 was found to be pH independent between 5 and 9.5 (Figure 5A), as it was reported for the wild-type protein (19).

This first intermediate decayed mono-exponentially on the millisecond time scale (0.4-10 ms) with a k_2 value independent of the protein concentration (data not shown). As reported for the wild-type protein, in the E114A mutant k_2 is directly proportional to H^+ concentration between pH 5 and 8 (Figure 5B), with $\log k_2 = \log k_0 - (0.80\pm0.1)\times pH$. A slope close to unity (i.e. 0.8±0.1) indicates that, like the wild-type protein (19), the decay of the first intermediate involves a single protonation process as the rate limiting step, the proton being directly provided by the bulk aqueous solvent. However, between pH 5 and 8, k_2 values determined for the E114A mutant are 10 times smaller than that of the wild-type protein (Figure 5B). This is reflected by the k_0 value, the limit of the protonation rate constant when pH values approach zero, calculated to be $(1.7\pm0.6)\times10^8$ M^{-1} s^{-1} for the E114A mutant and $(1.4\pm0.7)\times10^9$ M^{-1} s^{-1} for the wild-type protein (Figure 5B and Ref 19). These data show that the E114A mutation results in a decrease of the rate of protonation of the first reaction intermediate.

Above pH 8.4 and up to pH 9.5, in contrast with the wild-type protein, k_2 values for the E114A mutant became pH-independent (Figure 5B). Similar behavior at basic pH values was also described for the wild-type SORs from *Desulfovibrio vulgaris* (18) and *Archaeoglobus fulgidus* (20, 21) and was proposed to be associated with a protonation event arising from a water molecule instead of H_3O^+ at more acidic pH values (20, 21). This behavior could be also associated with the presence of a protonated base close to the active site. In the wild-type SOR from *D. baarsii*, where such pH dependent process was observed up to pH 10, this protonated base might be not be effective enough to out-compete the protonation process from the bulk solvent. For the E114A mutant, at basic pHs, the situation could be the opposite, due to the slower protonation process arising from the bulk.

The UV-vis absorption spectrum of the first reaction intermediate for the E114A mutant

was reconstructed from the absorbances at different wavelengths obtained after 50 µs of the reaction at pH 7.6 (data not shown). This spectrum exhibits a maximum at 610 nm and is identical to the spectrum of the first reaction intermediate reported for the wild-type protein, which was associated with a Fe^{3+}-peroxo species (19). Such a species results from the fast binding, at the sixth coordination position, of the superoxide anion and its subsequent reduction by the ferrous iron.

The spectrum of the second intermediate of the E114A mutant was reconstructed at pH 7.6, where k_2 exhibits a direct dependence with H^+ concentration and at pH 9.1, where k_2 was found to be pH independent (Figure 6). Both reconstructed spectra are similar and comparable to that determined for the second reaction intermediate in the wild-type protein (19), with a relatively narrow absorption band centered at 625 nm. This second intermediate, resulting from the protonation of the Fe^{3+}-peroxo species was proposed to be a Fe^{3+}hydroperoxo species (19).

As previously described (19), with our instrumental device, we are not able to follow the reaction kinetics above 30 ms, a time range in which the last step of the reaction is expected to occur (Scheme 1). This last step would correspond to the dissociation of the second reaction intermediate, the release of H_2O_2 and formation of the Fe^{3+} active site species. Such a final reaction step is supported by the appearance at the end of the reaction of a UV-vis absorption spectrum characteristic of the oxidized active site (Figure 6, dotted line), which clearly differs from that of the second reaction intermediate. This final spectrum was obtained from γ-ray irradiation experiments, carried out under the same experimental conditions as pulse radiolysis. This spectrum corresponds to a stoichiometric oxidation of the SOR Center II (ε_{630nm} = 1,660 mM^{-1} cm^{-1}, at pH 7.6) by $O_2^{\bullet-}$.

Resonance Raman experiments. Stabilization of a Fe^{3+}-peroxo species on the active site.

Figure 7 shows the 15 K RR spectra of the wild-type and E114A mutant oxidized with K_2IrCl_6, excited using a 647.1 nm laser, in resonance with the S → Fe^{3+} charge transfer band of the active site (22, 23). The preresonance contributions from Center I (the Fe^{3+} rubredoxin-like center) have been subtracted, as previously described (23). The active site modes thus enhanced predominantly arise from the Fe^{3+}-S(Cys) moiety. The 299/316/323 cm^{-1} cluster of bands in the *D. baarsii* wild-type spectrum (Figure 7a) was attributed to primarily Fe^{3+}-S(Cys) stretching mode and bending mode contributions (23). Since the 299 cm^{-1} band is the most intense, it is most likely predominantly Fe^{3+}-S(Cys) stretching in character (23). The 742 cm^{-1} band was assigned to the S-C_β stretching mode of Cys116 and the weakly enhanced Fe^{3+}-N(His) stretching mode bands from the Fe^{3+}-coordinating histidine residues are seen at 216, 234 and 238 cm^{-1} (Ref 23 and Figure 7). For the K_2IrCl_6 oxidized proteins (Figure 7), mutation of the Glu114 residue significantly perturbs the active site vibrational modes associated with the cysteine ligand, as compared to wild-type. The 299/316/323 cm^{-1} cluster of bands (wild-type) is shifted to 291/313/323 cm^{-1} (E114A) indicating a general significant downshift of the Fe-S(Cys) stretching and bending modes for the E114A mutant, corresponding to a significant weakening of the S-Fe^{3+} bond for this mutant.

The C_β-S stretching frequency is sizably increased from 742 (wild-type) to 755 (E114A) cm^{-1} (Figure 7). These data indicate that the E114A mutation results in an increase in electron density in the S-C_β bond probably from a slight geometry change of the bond angle. The 357 cm^{-1} band (wild-type), also assigned to a cysteine deformation mode containing significant C-N character (23), is not sizably changed in the mutant E114A spectrum (i.e. 356 cm^{-1}). However, Figure 7 indicates some small but significant changes in some of the vibrational frequencies associated with the Fe-N modes of the Fe-coordinating histidine residues. For example the 216 cm^{-1} frequency in the wild-type spectrum shifts to 214 cm^{-1}. All the above observations clearly show that the E114A mutation results in localized structural changes primarily associated with Cys116, with a notable decrease of the strength of the S-Fe bond.

The treatment of SOR with a slight excess of H_2O_2 followed by rapid freezing was previously reported to form a metastable Fe^{3+}-peroxo species at the SOR active site, in particular when the oxidized active site sixth ligand was removed (i.e. the E47A mutation) (22, 23). These studies allowed a detailed resonance Raman characterization of a particular high-spin Fe^{3+} peroxo species

exhibiting $\nu(Fe^{3+}\text{-}O_2)$ and ν(O-O) stretching frequencies of 433-438 cm^{-1} and 850-852 cm^{-1}, respectively (22, 23). When the E114A mutant was similarly treated with 6 eq of H_2O_2 at pH 8.5 and rapidly frozen (less than 5 sec), the RR spectrum of the E114A mutant exhibited new bands at 446 and 851 cm^{-1} (Figure 8) that were not present in the spectrum of the K_2IrCl_6-oxidized protein (Figure 7). These band frequencies are consistent with the $\nu(Fe\text{-}O_2)$ and ν(O-O) stretching modes, respectively, of a Fe^{3+} peroxo species, as previously verified for the wild-type and E47A mutant of the SOR from *D. baarsii* using ^{18}O-labeling (22, 23). The intensities of these two bands are similar to that of the 756 cm^{-1} band (C-S stretching mode), a marker for the active site in the Fe^{3+} state, as reported for the E47A mutant (at 742 cm^{-1}) (Figure 8). For the wild-type protein, the two RR bands corresponding to the Fe^{3+}-peroxo species are very weak compared to the 742 cm^{-1} band (Figure 8 and Ref 23), indicating that this species is trapped to a lesser degree[1]. In contrast, for the E114A mutant, the intensities of the peroxo bands indicate that when treated with H_2O_2, this mutant trapped and stabilized by rapid freezing, a significant population of the Fe^{3+}-peroxo species at the active site, as was observed for the *D. baarsii* E47A mutant (22, 23). However, in the case of the E114A mutant, the $\nu(Fe\text{-}O_2)$ stretching mode is observed at a significantly higher frequency compared to the E47A mutant (446 cm^{-1} compared to 438 cm^{-1}, respectively), whereas the ν(O-O) stretching mode remains comparable (851 cm^{-1} for the E114A and 850 cm^{-1} for the E47A). These observations indicate that the Fe-O bond is stronger for the Glu114 mutant that it is for wild-type and E47A.

The low temperature EPR spectrum of a rapidly frozen solution of E114A mixed with H_2O_2 in conditions comparable to those of the RR samples corresponding to Figure 8, exhibits a feature at g = 4.3, similar to that observed for the K_2IrCl_6 oxidized protein (Figure 3). Except those for the iron corresponding to Center I which remained unchanged, no other signals were observed. This indicates that the peroxo species formed in these conditions is associated with a high spin rhombic ferric ion.

Altogether these results indicate that, like the E47A mutant, the E114A mutation strongly stabilizes a high spin Fe^{3+} peroxo species in its active site. However, the Fe-O bond of the peroxo is significantly strengthened in the E114A mutant.

Effects of the E114A mutation on the cellular activity of SOR.

Turnovers of SOR with $O_2^{\bullet-}$ have been described using NADPH reductase as a source of electrons to regenerate the active SOR ferrous state and xanthine oxidase as a source of $O_2^{\bullet-}$ (31). Using the NADPH flavodoxin reductase from *E. coli* (Fpr) as a source of electron, we have observed oxidation of NADPH specifically associated with turnovers of SOR with $O_2^{\bullet-}$ (Supplemental Data, Figure 1). An NADPH:superoxide oxidoreductase activity for the wild type SOR of 9 μM $NADPH_{ox}$/min was determined. The E114A mutation does not modify the NADPH :superoxide oxidoreductase activity of the protein (Supplemental Data, Figure 1). As shown previously (31), under these conditions, the $O_2^{\bullet-}$ flux is the rate limiting process for NADPH consumption. Consequently this test does not provide additional information on the effects of the E114A mutation on the subsequent steps after $O_2^{\bullet-}$ binding at the SOR active site. However it demonstrates that turnovers still occur with this mutant.

The ability of the SOR E114A mutant protein to complement *E.coli* SOD deficiency was tested as described in (16). The *E.coli sodA sodB recA* mutant cannot grow in the presence of oxygen because of the combined lack of superoxide dismutase activity (*sodA sodB*) and the DNA strand break repair activity (*recA*) that results in lethal DNA oxidative damage. As shown in Table I, at low IPTG concentration, the production of the E114A mutant SOR protein restored only 23% of the aerobic growth of *sodA sodB recA* mutant, whereas the wild type SOR protein restored 42 %. At higher IPTG concentration, 58% of anaerobically growing *E. coli* cells producing the E114A SOR were able to grow aerobically compared to 78% for those producing wild type SOR. These data indicate that production

[1] This has been quantitatively confirmed using Mossbauer spectroscopy (24). Thus, despite variations in the UV-vis absorption band maxima of the wild-type, E47A and E114A SORs, the relative intensities of the RR bands corresponding to the Fe^{3+}-peroxo species qualitatively reflect the degree of trapping of this species.

of E114A SOR can compensate for SOD deficiency in *E. coli*, but with significantly less efficiency than the wild-type SOR.

DISCUSSION

The presence of a cysteine axial ligand in the SOR iron active site has long been proposed to be an essential feature in the reactivity of the enzyme with superoxide (5, 8). For heme-thiolate proteins like cytochrome P450 and for [Fe-S] cluster proteins (27-29), it has been proposed that H-bonds on the cysteine ligand would change the strength of the S-Fe bond and therefore modulate the chemistry of these proteins. A similar situation is expected for SOR where such changes in the S-Fe bond should play some role in modulating the reactivity of SOR with superoxide. Since it is *trans* to the superoxide binding site, the cysteine ligand should play a critical role in donating electron density to the iron metal center so as to promote $Fe^{2+} \rightarrow$ superoxide electron transfer, or H_2O_2 dissociation from high-spin Fe^{3+}, or both. In particular for SOR, in the well conserved tetrapeptide Cys116-Asn117-Leu/Ile118-His119, two peptide NH groups from the Leu/Ile118 and His119 are within H-bonding distance of the Cys116 ligand sulfur ((Figure 1, (14)). Furthermore, for the *D. baarsii* enzyme, as previously suggested (26) and confirmed here by FTIR measurements, the carboxylic group of the Glu114 side chain, which directly faces the S-Fe bond at about 5-6 Å from both atoms, is in interaction with the iron atom in the active site (Figure 1). Glu114 is well conserved in the two-iron SORs, whereas it is replaced by a Ser residue in the one-iron type of SORs, such as the *P. furiosus* enzyme (7).

In this work, we have mutated the Glu114 residue of the SOR from *D. baarsii*, into alanine. The data reveal that the presence of the Glu114 carboxylic group allows a fine tuning of the S-Fe bond strength, which appears to be a determining factor in the rate of formation and release of the reaction product, H_2O_2.

The pulse radiolysis experiments presented here showed that the E114A mutation does not change the overall reaction mechanism of SOR with superoxide (Scheme 1) and still reacts very rapidly with superoxide. Although with our pulse radiolysis apparatus we were not able to kinetically characterize the final step of the catalytic cycle (formation of H_2O_2 and the resting ferric active site), this final step does exist for the E114A mutant (Figure 6), as it does for wild-type and other mutants we have studied (16, 19).

However, we have observed that the mutation specifically decreases by a factor of 10 the rate constant for the protonation process of the Fe^{3+}-peroxo intermediate species, to form the Fe^{3+}-hydroperoxo intermediate species. An interpretation for this very specific effect is not obvious at first glance. In fact, since the Glu114 is located on the opposite side to the intermediate peroxo adducts (Figure 1) and that, as seen here by FTIR spectroscopy, the E114A mutation does not induce marked global structural changes in the protein, the decrease of the protonation rate of the peroxo species is not expected to result from structural constraints that could appear in the active site. Also, the mutation does not apparently modify the proton source, since as in the wild-type protein, the proton is still provided directly by the bulk solvent (Figure 5). Consequently, this slower protonation process could be associated with some changes in the intrinsic properties of the Fe^{3+}-peroxo intermediate species. Interestingly, the E114A mutation removes the dipolar interaction with Cys116 (Figure 4) as well as potentially removing an H-bond with the backbone C=O group of His49 whose side chain is ligated to the Fe atom (Figure 1). All these factors could affect the local electrostatics around the Cys-Fe moiety as well as slightly altering its bonding geometry, distance, and therefore the bond strength.

Several arguments reported here are in agreement with the above proposals.

First, we previously reported that the wild-type protein exhibits an alkaline transition of the $S \rightarrow Fe^{3+}$ charge transfer UV-vis absorption (644 to 560 nm, Δ = 84 nm, pK_a = 9.0), which has been attributed to the displacement of the Glu47 ligand by OH^- at basic pH values (8, 24). This results in an increase in the electron density at the Fe^{3+} site (25). The E114A mutant exhibits a similar alkaline transition with similar pK_a and magnitude values (pK_a = 8.8 and Δ = 85 nm). However, the mutation induces spectral blue-shifts of 12-13 nm for both the Fe^{3+}-Glu47 and Fe^{3+}-OH ligated states (632 to 547 nm, respectively). The significantly different $S \rightarrow Fe^{3+}$ charge transfer absorption maxima of the E114A indicates localized changes at the

active site which affect electron density at the high spin Fe^{3+} atom (8).

Second, the RR spectra show that the E114A mutation has very specific effects on the cysteine ligand (Figure 7). When compared to the wild-type and the E47A proteins, the E114A mutation induces a significant weakening of the S-Fe^{3+} bond (299/316/323 to 291/313/311 cm^{-1}) and a concomitant strengthening of the C-S bond (743 to 756 cm^{-1}) of the cysteine ligand. These localized structural changes are compatible with the observed blue shift (12-13 nm) of the S → Fe^{3+} charge transfer band of the oxidized iron site in the E114A mutant.

From these data, one can conclude that the carboxylic side chain of Glu114, which faces directly the S-Fe bond at about 5-6 Å distances of both atoms, allows a fine tuning of the strength of the S-Fe bond. In particular it induces a strengthening of the S-Fe bond.

Such an effect should have consequences on the bonding of the Fe^{3+}-peroxo intermediates that form during the reaction with superoxide. Up to now, the reaction of SOR with H_2O_2 is the only way that has been reported to allow a detailed characterization by resonance Raman of a Fe^{3+}-peroxo species in the active site of SOR (23, 24). Although it is not known yet if such a peroxo species is identical to the ones formed during the reaction of the protein with superoxide, the characterization of a Fe^{3+}-peroxo species here and elsewhere in SORs by resonance Raman are most likely informative with respect to the properties of the intermediates species formed in the reaction with superoxide. In support of that, it has been recently reported that the iron complex SOR mimic $[Fe^{II}(cyclam)\text{-}PrS]^+$, when reacted with superoxide, forms an high-spin iron peroxo intermediate with Fe-O and O-O resonance Raman bands (32) very similar to those observed for the SOR protein treated with H_2O_2 (23, 24).

When the E114A mutant is reacted with a slight excess of hydrogen peroxide, we showed that it stabilizes an iron peroxo species at its active site, which can be freeze-trapped and characterized by resonance Raman spectroscopy. The RR spectrum exhibits intense $\nu(Fe\text{-}O_2)$ and $\nu(O\text{-}O)$ mode bands, at 446 and 851 cm^{-1}, respectively, characteristic of the ferric iron peroxo species similarly trapped in other SORs and which has been assigned to a side-on high-spin Fe^{3+}-peroxo species (22, 23). EPR experiments presented here show that the peroxo species in the E114A mutant is also associated with a high-spin ferric iron site.

Such a high-spin iron peroxo species was readily trapped and characterized in another *D. baarsii* SOR variant, the E47A mutant protein (22, 23). In the wild-type protein, a similar peroxo species, with RR band frequencies identical to those of the E47A mutant, was also observed but was trapped to a much lesser degree. This is consistent with the fact that the wild-type SOR active site accommodates such species only transiently since the Glu47 residue binds to the sixth coordination position of the Center II ferric site, facilitating H_2O_2 release by a ligand exchange mechanism (23). Thus, for the E47A mutant, the stabilization of the peroxo species was associated with the presence of the alanine residue incapable of ligating to the ferric iron (23). Accordingly, in the E47A mutant, the Fe-O and O-O stretching modes exhibited identical vibrational frequencies as those of the wild-type protein (Figure 8 and Refs 22, 23). Interestingly, the ν(Fe-O) band of the iron peroxo species in the E114A mutant is shifted to higher frequency (446 compared to 438 cm^{-1} in the wild-type and E47A proteins), whereas the ν(O-O) bands exhibit comparable frequencies (850-851 cm^{-1}). This indicates that the Fe-O bond is stronger in the E114A mutant than in the E47A and wild-type proteins. A stronger Fe-O bond is in good agreement with the stabilization of the peroxo species in the E114A mutant protein. Thus, the mechanism by which the E47A and E114A mutants induce a stabilization of the peroxo species appears to be fundamentally different.

For the E114A mutant, the strengthening of the Fe-O bond correlates well with the observed weakening of the S-Fe bond which indicates a decreased electron donation from the cysteine ligand to the iron. For a high-spin Fe^{3+}-peroxo side-on bonding situation, the in-plane π^* orbital of the peroxo ligand overlaps with the Fe^{3+} d_{xz} orbital (23 and references therein). Thus any electron density donation to the filled π^* orbital, from the iron center and originating from cysteine ligand in the trans position, is expected to weaken the Fe-O_2 bond. The weaker S-Fe^{3+} bond in the E114A mutant (compared to wild-type) indicates decreased cysteinate electron donating power to the iron and the peroxo π^* orbital, and

therefore a stronger Fe-O_2 bond (compared to wild-type) is expected, and indeed observed[2].

The strengthening of the Fe-O bond of the Fe^{3+}-peroxo species observed in the E114A mutant, with no modification of the strength of the O-O bond is expected to change the acidity of the peroxo species, most likely increasing it. Interestingly, the Brönsted catalysis equation predicts that among a series of bases, the logarithm of the rate constant of protonation of a species is directly proportional to its pK_a value. This appears to be in very good agreement with the decrease of the rate of the protonation of the Fe^{3+}-peroxo species intermediate observed in the reaction of the E114A mutant with superoxide (Figure 5, decreases of k_2 value, Scheme 1). Thus, the properties of the peroxo species characterized by RR from the reaction of SOR with H_2O_2 account well for the specific effect of the E114A mutation on the protonation rate of the first reaction intermediate during the reaction with superoxide. Thus, we propose that the decrease of this protonation rate can be directly associated with a decrease of the pK_a value of the peroxo intermediate, which as discussed above, originates from the strengthening of the Fe-O (peroxo) bond in that mutant.

Using the Fpr reductase from *E. coli* as a source of electrons for SOR, we showed that the E114A mutation did not inhibit turnovers with $O_2^{\bullet-}$. However, in cellular conditions, the complementation of an *E. coli sod* mutant strain with the *D. baarsii sor* gene was significantly impaired by the E114A mutation.

Altogether with our previous conclusions that the E114A mutant stabilizes a peroxide intermediate in its active site, these data suggest that an efficient release of the peroxide intermediate to form H_2O_2 is important for the SOR detoxification activity.

In conclusion, these data highlight a functional role for the carboxylic side chain of Glu114 in the SOR from *D. baarsii*. This carboxylic group, which is in interaction with the S-Fe bond, directly contributes to a fine tuning of the S-Fe strength. The data obtained with the E114A mutant allow to gauge the importance of the strength of the S-Fe bond in the reaction with superoxide, which appear to directly affect both the strength of the Fe-O bond and the pK_a values of the iron peroxo intermediate that is formed during catalysis. Both factors are essential in the formation of the reaction product H_2O_2, which in SOR arises from protonations of the peroxo intermediate and cleavage of the Fe-O bond. One should note that a strengthening of the Fe-O bond in the E114A mutant should also markedly affect the last step of the reaction cycle with superoxide. This final step, not investigated yet, presumably involves a second protonation process at the level of the Fe^{3+}-hydroperoxide intermediate together with the cleavage of the Fe-O bond to form and release H_2O_2 (Scheme 1). Further studies are needed to specify this point.

P450 enzymes like SOR form Fe^{3+} peroxide intermediate species with a *trans* cysteinate ligand during their catalytic cycles. However, at the difference of the P450 enzymes which favor the heterolytic cleavage of the O-O bond of the peroxide intermediate to form the high valent iron oxo species (33), our previous RR experiments demonstrated that the SOR active site can accommodate unusual Fe^{3+}-peroxo species with particularly weak Fe-O bond and strong O-O bond, which, in addition to the spin state of the iron (34), clearly favors the Fe-O bond cleavage to form its reaction product H_2O_2. Our present work further shows that the strength of the S-Fe bond, which is finely tuned by the cysteine environment, significantly contributes to this unusual weak Fe-O bond in SOR.

Very recently, the stabilization of peroxide intermediate in the E114A mutant has allowed the determination of a high resolution structure of three slightly different conformations of iron peroxide intermediates in the SOR active site (35). These studies highlight a specific protonation mechanism of the Fe-OOH on the proximal oxygen to release H_2O_2. This provides additional important data that account for the differences in the evolution of the Fe^{3+}-peroxide species between SOR and P450 enzymes.

[2] A similar *trans* ligand electron donation effect are expected for end-on high-spin Fe^{3+}-OO(H) hydroperoxo species. For example, SOR model complexes with apical ligands with decreased Lewis basicity (i.e. decreased electron density donation) result in end-on high-spin Fe^{3+}-alkylperoxo species with increased Fe-O bond strengths and stability (34). Thus, the arguments also qualitatively apply to a possible end-on Fe^{3+}-(hydro)peroxo that could form in the SOR catalytic reaction with superoxide.

REFERENCES

1. Jenney, F. E. Jr., Verhagen, M. F. J. M., Cui, X., and Adams, M. W. W. (1999) *Science* **286**, 306-309
2. Lombard, M., Fontecave, M. Touati, D., and Nivière, V. (2000) *J. Biol. Chem.* **275**, 115-121
3. Nivière, V., and Fontecave, M. (2004) *J. Biol. Inorg. Chem.* **9**, 119-123
4. Kurtz, D. M. Jr. (2004) *Acc. Chem. Res.* **37**, 902-908
5. Brines, L. M., and Kovacs, J. A. (2007) *Eur. J. Inorg. Chem.* **1**, 29-38
6. Valentine, J. S., Wertz, D. L, Lyons, T. J., Liou, L. L., Goto, J. J., and Gralla, E. B. (1998) *Curr. Opin. Chem. Biol.* **2**, 253-262
7. Andrew, P. Y., Hu, Y., Jenney, F. E. Jr., Adams, M. W. W., and Rees, D. C. (2000) *Biochemistry* **39**, 2499-2508
8. Clay, M. D., Jenney, F. E. Jr., Hagedoorn, P. L., George, G. N., Adams, M. W. W., and Johnson, M. K. (2002) *J. Am. Chem. Soc.* **124**, 788-805
9. Lombard, M., Touati, D., Fontecave M., and Nivière, V. (2000) *J. Biol. Chem.* **275**, 27021-27026
10. Jovanovic, T., Ascenso, C., Hazlett, K. R. O., Sikkink, R., Krebs, C., Litwiller, R., Benson, L. M., Moura, I., Moura, J. J. G., Radolf, J. D., Huynh, B. H., Naylor, S., and Rusnak, F. (2000) *J. Biol. Chem.* **275**, 28439-28448
11. Abreu, I. A., Saraiva, L. M., Carita, J., Huber, H., Stetter, K. O., Cabelli, D. E., and Teixeira, M. (2000) *Mol. Microb.* **38**, 322-334
12. Santos-Silva, T., Trincao, J., Carvalho, A. L., Bonifacio, C., Auchère, F., Raleiras, P., Moura, I., Moura, J. J. G., and Romao, J. (2006) *J. Biol. Inorg. Chem.* **11**, 548-558
13. Coelho, A., Matias, P., Fülöp, V., Thompson, A., Gonzalez, A., and Carrondo, M. A. (1997) *J. Biol. Inorg. Chem.* **2**, 680-689
14. Adams, V., Royant, A., Nivière, V., Molina-Heredia, F.P., and Bourgeois, D. (2004) *Structure* **12**, 1729-1740
15. Emerson, J. P., Cabelli, D. E., and Kurtz, D. M. Jr., (2003) *Proc. Natl. Acad. Sci. U.S.A.* **100**, 3802-3807
16. Lombard, M., Houée-Levin, C., Touati, D., Fontecave, M., and Nivière, V. (2001) *Biochemistry* **40**, 5032-5040
17. Nivière, V., Lombard, M., Fontecave, M., and Houée-Levin, C. (2001) *FEBS Lett.* **497**, 171-173
18. Emerson, J. P., Coulter, E. D., Cabelli, D. E., Phillips, R. S., and Kurtz, D. M. Jr. (2002) *Biochemistry* **41**, 4348-4357
19. Nivière, V., Asso, M., Weill, C.O., Lombard, M., Guigliarelli, B., Favaudon, V., and Houée-Levin, C. (2004) *Biochemistry* **43**, 808-818
20. Rodrigues, J. V., Abreu, I. A., Cabelli, D., and Teixeira, M. (2006) *Biochemistry* **45**, 9266-9278
21. Rodrigues, J. V., Abreu, I. A., Cabelli, D., and Teixeira, M. (2006) *J. Biol. Inorg. Chem.* In press, published online 26 Oct 2006
22. Mathé, C., Mattioli, T. A., Horner, O., Lombard, M., Latour, J. M., Fontecave, M., and Nivière, V. (2002) *J. Am. Chem. Soc.* **124**, 4966-4967
23. Mathé, C., Nivière, V., and Mattioli, T. A. (2006) *Biophys. Chem.* **119**, 38-48
24. Horner, O., Mouesca, J. M., Oddou, J. L., Jeandey, C., Nivière, V., Mattioli, T. A., Mathé, C., Fontecave, M., Maldivi, P., Bonville, P., Halfen, J. A., and Latour, J. M. (2004) *Biochemistry* **43**, 8815-8825
25. Mathé, C., Nivière, V., and Mattioli, T. A. (2005) *J. Am. Chem. Soc.* **127**, 16436-16441
26. Berthomieu, C., Dupeyrat, F., Fontecave, M., Verméglio, A., and Nivière, V. (2002) *Biochemistry* **41**, 10360-10368
27. Poulos, T. L. (1996) *J. Biol. Inorg. Chem.* **1**, 356-359
28. Dey, A., Okamura, T., Ueyama, N., Hedman, B., Hodgson, K. O., and Solomon, E. I. (2005) *J. Am. Chem. Soc.* 1**27**, 12046-12053

29. Lin, I.-J., Gebel, E. B., Machonkin, T. E., Westler, W. M., and Markley, J. (2005) *Proc. Natl. Acad. Sci. U.S.A.* **102**, 14581-14586
30. Clay, M. D., Emerson, J. P., Coulter, E. D., Kurtz, D. M. Jr., and Johnson, M. K. (2003) *J. Biol. Inorg. Chem.* **8**, 671-682
31. Emerson, J. P., Coulter, E. D., Phillips, R. S., and Kurtz, D. M. Jr. (2003) *J. Biol. Chem.* **278**, 39662-39668
32. Kitagawa, T., Dey, A., Lugo-Mas, P., Benedict, J. B., Kaminsky, W., Solomon, E., and Kovacs, J. A. (2006) *J. Am. Chem. Soc.* 1**28**, 14448-14449
33. Denisov, I. G., Makris, T. M., Sligar, S. G., and Schlichting, I. (2005) *Chem. Rev.* **105**, 2253-2277
34. Bukowski, M. R., Halfen, H. L., van den Berg, T. A., Halfen, J. A., and Que, L. (2005) *Angew. Chem. Int. Ed.* **44**, 5483-5484
35. Katona, G., Carpentier, P., Nivière, V., Amara, P., Adam, V., Ohana, J., Tsanov, N. and Bourgeois, D. (2007) *Science* , in press

FOOTNOTES

* We acknowledge Dr. Vincent Favaudon for assistance with pulse radiolysis experiments, Dr. Stéphane Ménage for assistance with EPR spectroscopy and Dr. Danièle Touati for her help in *E. coli* complementation tests. This work was supported by grants from the CEA, programme "Toxicologie Nucléaire" (V.N. and C.B.). C.O.W. acknowledges a Post-doctoral fellowship from the CEA program "Toxicologie Nucléaire".
Abbreviations. SOR, superoxide reductase; FTIR, Fourier transform infrared; RR, resonance Raman; EPR, electron paramagnetic resonance; Fpr, flavodoxin reductase from *Escherichia coli*.

FIGURE LEGENDS

Figure 1. Active site of the SOR from *Desulfoarculus baarsii* from its crystal structure at 1.15 Å resolution (14). Hydrogen bonds are shown in red: i) between the NH main chains of Ile118 (3.41 Å), His119 (3.26 Å) and the sulphur atom of the Cys116; ii) one oxygen atom of the Glu114 side chain is located at 2.63 Å from the backbone C=O of His49. This is consistent with a protonated Glu114 carboxylate side chain forming a H-bond with the backbone CO of His49. In black are shown the distances between the two oxygen atoms of the carboxylic side chain of Glu114 and the sulphur and iron atoms (5.6-6.5 Å).

Figure 2. pH dependence of the light absorption spectra of the oxidized SOR from *D. baarsii* E114A mutant active site. The as isolated enzyme (61.3 µM in 10 mM of the different buffers) was oxidized with a slight excess of K_2IrCl_6 and the spectra were recorded immediately. The spectra were corrected from the absorbances of Center I. (A) pH 5.0 (○), pH 6.5 (●), pH 7.5 (△), pH 8.1 (▲), pH 8.5 (□), pH 9.1 (■), pH 9.5 (▽) and pH 10.2 (▼). The insets show the pH dependence of the absorbance at 660 nm. The titration curve fitted the equation expected from a single protonation process, $A_{660} = (A_{660max} + A_{660min} \times 10^{(pH-pKa)})/(1 + 10^{(pH-pKa)})$. A pK_a value of 8.8±0.1 was determined.

Figure 3. EPR spectra of the SOR from *D. baarsii* E114A mutant. The mutant protein (200 µM in 10 mM Tris-HCl buffer pH 8.5) was oxidized with (a) three equivalents of K_2IrCl_6, (b) 6 equivalents of H_2O_2 (incubation time 15 s and freezing). EPR conditions: temperature, 4.2 K; microwave power 25 mW at 9.447 GHz; modulation amplitude, 20 G at 100 kHz.

Figure 4. Reduced *minus* oxidized FTIR difference spectra of the SOR active site wild-type (thin line) and E114A mutant (thick line) from *D. baarsii*. Potentials of 650 mV and 250 mV (versus NHE) were applied at the working electrode to obtain the oxidized and reduced states, respectively. The spectra

consist of an average of data recorded on 30 electrochemical cycles, 300 scans per cycle, 4 cm^{-1} resolution.

Figure 5. pH-dependence of rate constants k_1 and k_2 for the reaction of SORs from *D. baarsii* (100 µM) with $O_2^{\bullet-}$ (3 µM), generated by pulse radiolysis. (A) SOR E114A mutant. k_1 did not vary significantly with pH. (B) (○) SOR E114A mutant. Between 5.2 <pH< 8.5, k_2 values were fitted to a linear equation, log k_2 = log k_0 - αpH, with α = 0.8±0.1 and k_0 = 1.7±0.6x10^8 M^{-1} s^{-1}. (●) SOR wild-type protein, shown for comparison. k_2 values were fitted to a linear equation, log k_2 = log k_0 - αpH, with α = 0.80±0.05 and k_0 = 1.4±0.7x10^9 M^{-1}.

Figure 6. Transient absorption spectra (in a 2 cm path-length cuvette) of the second reaction intermediates formed upon the reaction of the E114A SOR mutant (100 µM) with $O_2^{\bullet-}$ (3 µM), generated by pulse radiolysis at different pHs. (○) pH 9.1, 10 ms after the pulse. (●) pH 7.6, 10 ms after the pulse. The dotted lines show the absorption spectrum of the iron center II of the E114A mutant (3 µM, pH 7.6) after complete oxidation by 3 µM of $O_2^{\bullet-}$ generated by γ–ray irradiation in the presence of a catalytic amount of catalase, or by reaction with a slight excess of K_2IrCl_6.

Figure 7. Low temperature (15 K) resonance Raman spectra of the SOR active site wild-type and E114A mutant from *D. baarsii* oxidized with 3 eq of K_2IrCl_6 excited at 647.1 nm. (a) E114A mutant (b) Wild-type. SOR concentration was 3 mM in 100 mM Tris-HCl buffer pH 8.5; laser power was 30 mW at the sample; spectral resolution was <3 cm^{-1}. Contribution of the Fe^{3+} rubredoxin-like center (Center I) and the ice were subtracted from each spectrum (23).

Figure 8. Low temperature (15 K) resonance Raman spectra of the SOR active site wild-type, E47A and E114A mutants from *D. baarsii* oxidized with 6 eq of H_2O_2 excited at 647.1 nm. (a) E114A mutant (b) E47A mutant and (c) Wild-type. SOR concentration was 3 mM in 100 mM Tris-HCl buffer pH 8.5; laser power was 30 mW at the sample; spectral resolution was <3 cm^{-1}. Contribution of the Fe^{3+} rubredoxin-like center (Center I) and the ice were subtracted from each spectrum (23). The 230 cm^{-1} band is due to ice contributions.

Table I. Aerobic survival of SOD-deficient *E. coli* cells depending on their production of wild-type or E114A mutant of SOR.[a]

plasmid	Aerobic survival (%)[b]	
	[IPTG]	
	5 µM	1 mM
pJF119EH (control vector)	0.003	nd
pMJ25 (SOR wild-type)	42±5	78±6
pCWE114A (SOR E114A)	23±3	58±3

[a] Anaerobic cultures of *sodA sodB recA E.coli* mutant QC 2375 transformed with pJF119EH, pMJ25 or pCWE114A were plated on LB medium plus 5 µM or 1 mM IPTG, under anaerobic and aerobic conditions. Colonies were counted and after 24 h incubation at 37 °C.

[b] Survival was calculated as the ratio of the number of colonies under aerobic conditions to those under anaerobic conditions. Values are the means of five experiments. 100% corresponds to 1.8-2.3 10^8 colonies. nd, not determined.

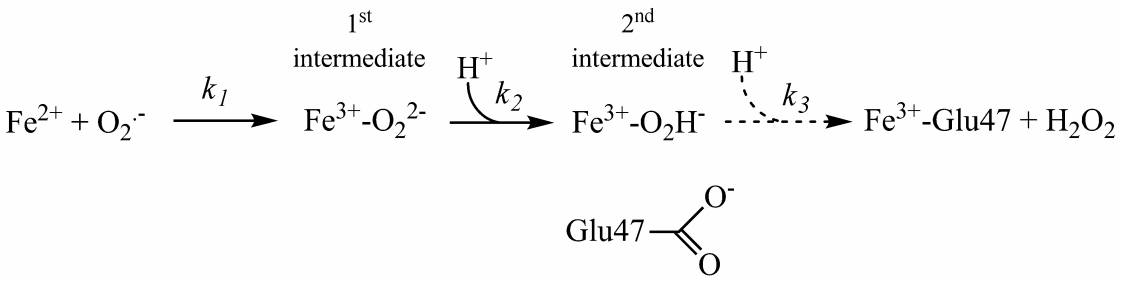

Scheme 1. Reaction mechanism of the SOR from *D. baarsii* with $O_2^{\bullet-}$ (from Ref 19).

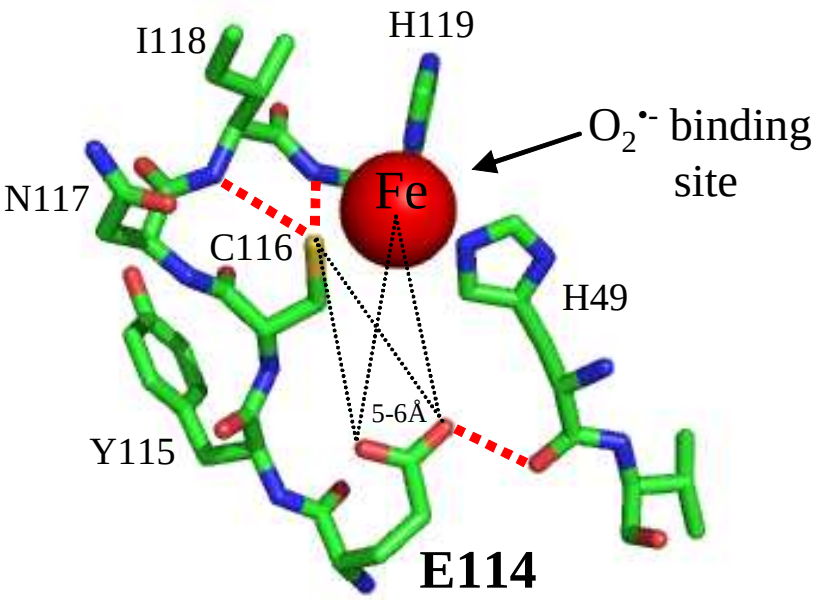

Figure 1

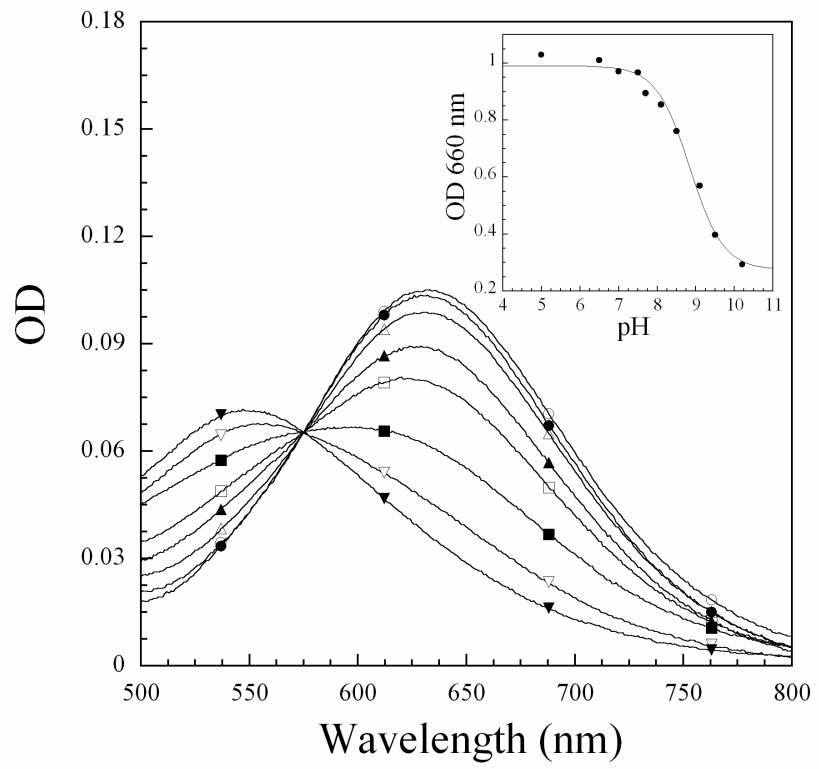

Figure 2

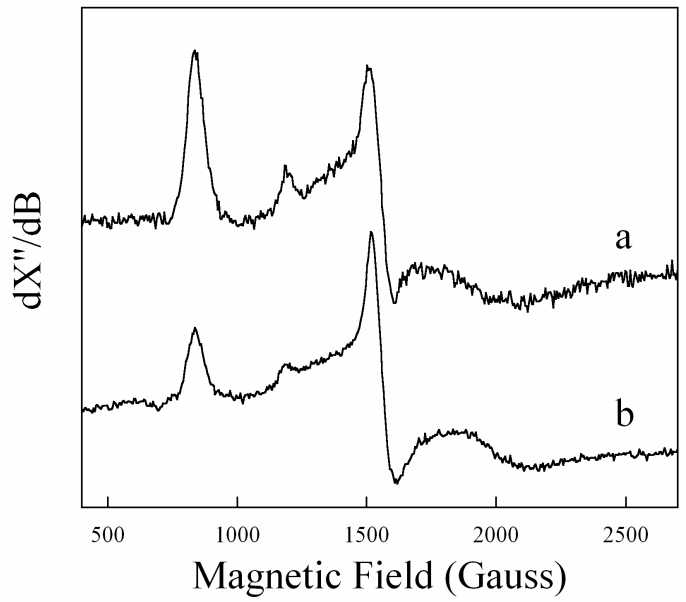

Figure 3

Figure 4

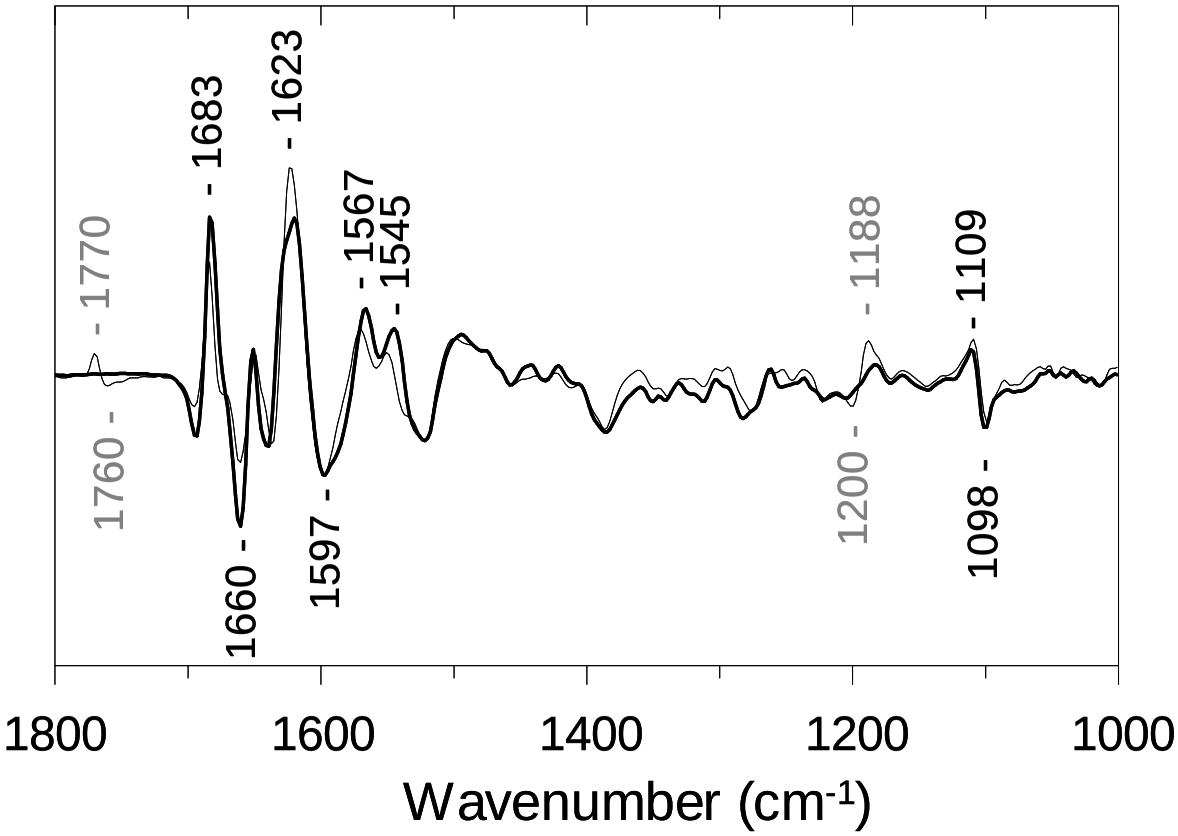
- 1770
- 1683
- 1623
- 1567
- 1545
- 1188
- 1109
1760 -
1660 -
1597 -
1200 -
1098 -
1800
1600
1400
1200
1000
Wavenumber (cm-1)

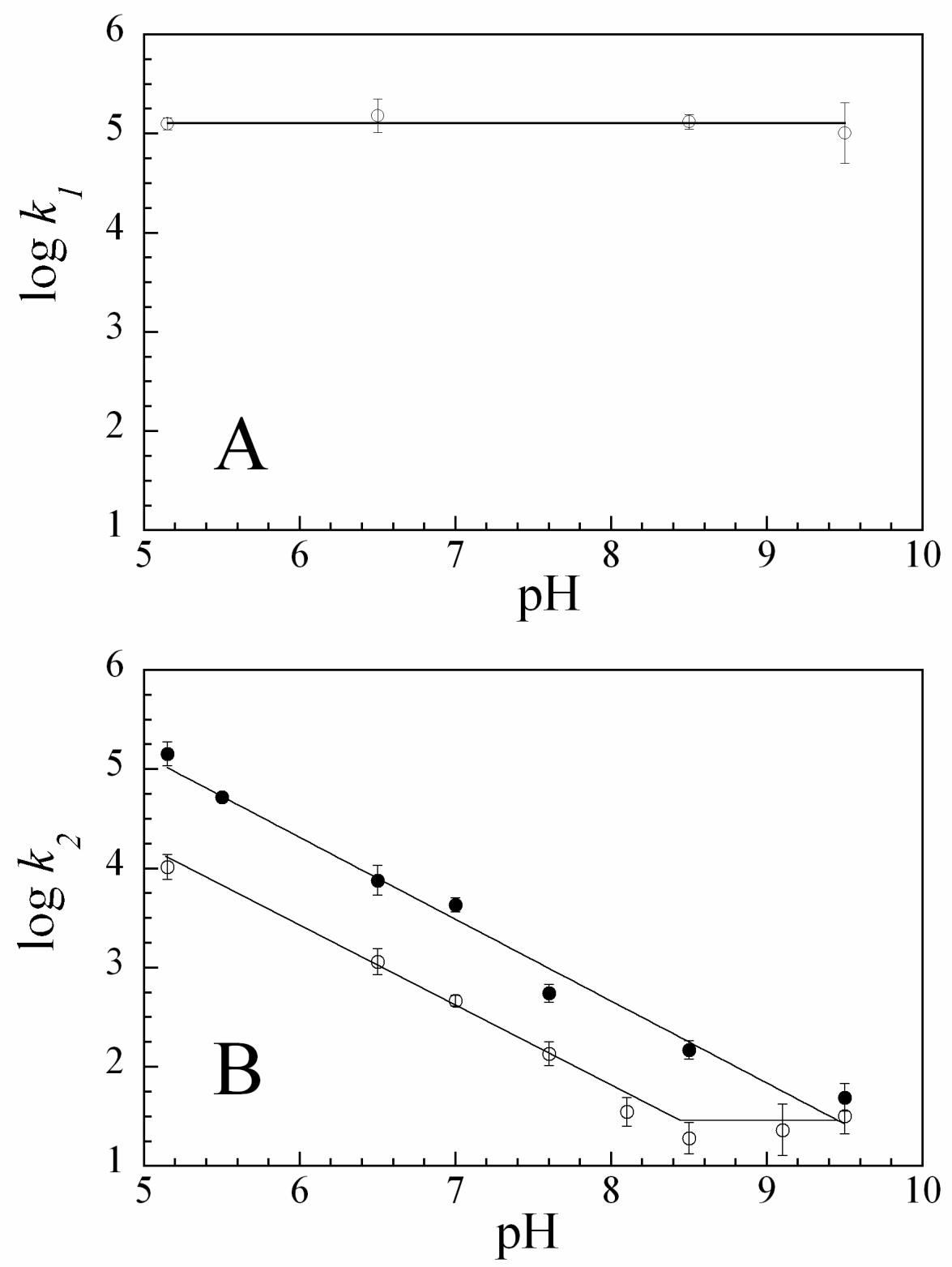

Figure 5

Figure 6

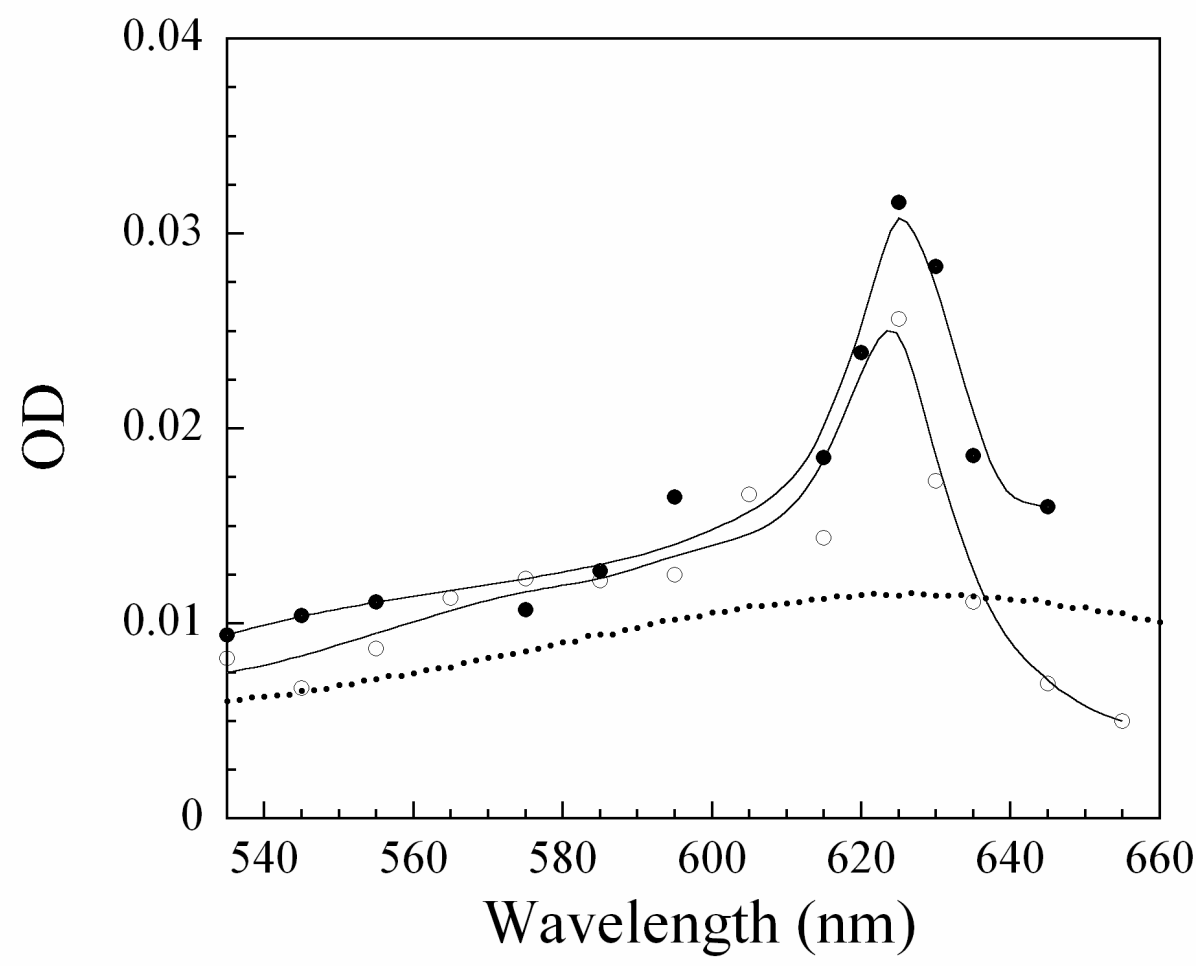

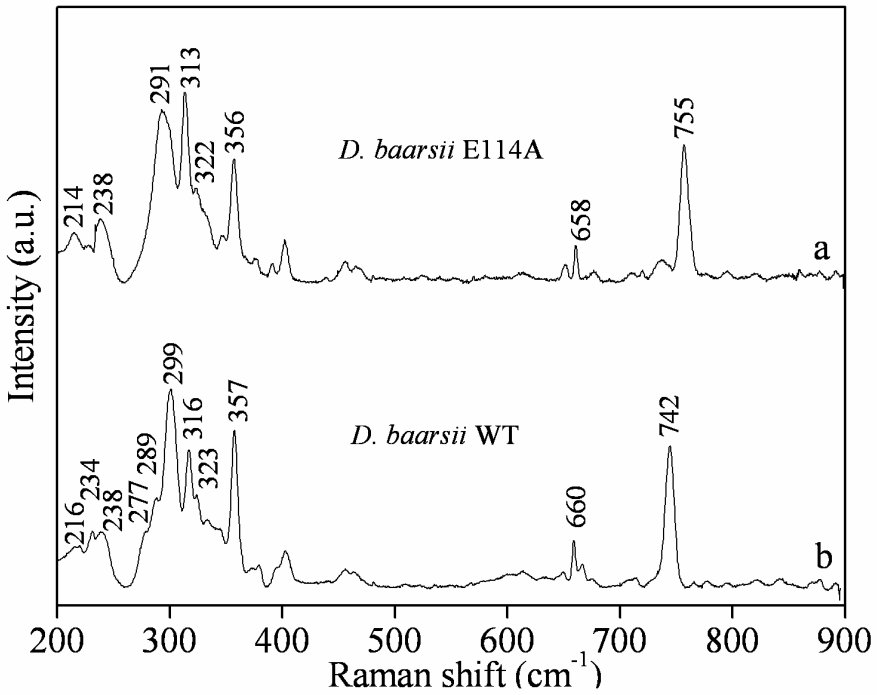

Figure 7

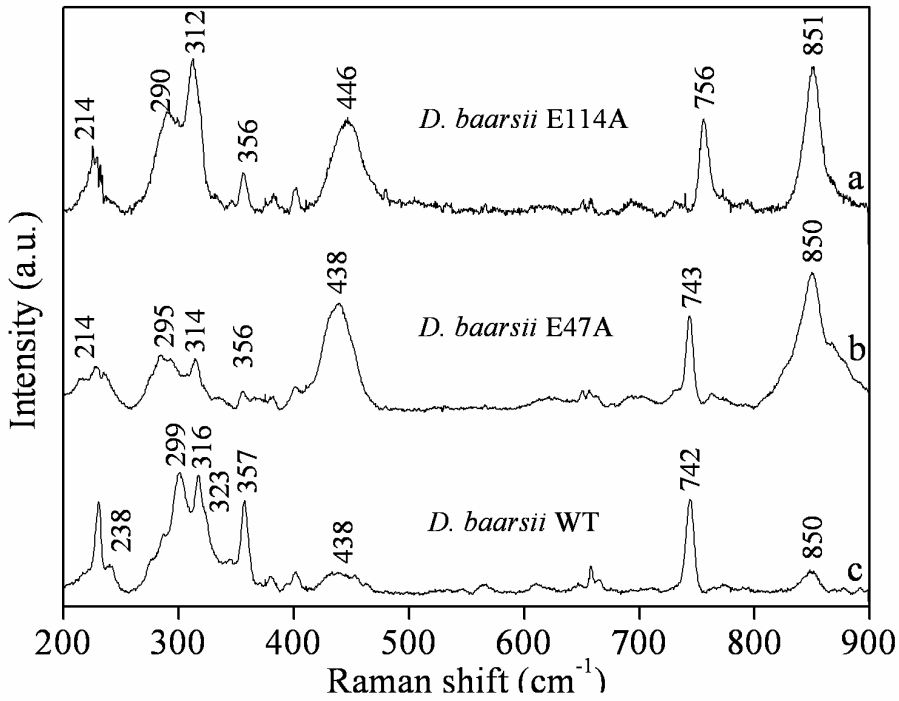

Figure 8